Experimental investigations on the mechanical properties and damage detection of carbon nanotubes modified crumb rubber concrete

Suliman Khan [a], Shahzad Ashraf [b,*], Shehroze Ali [a,c], Khushal Khan [a]

[a] *Department of Civil Engineering, NFC Institute of Engineering and Fertilizer Research (IE&FR), Faisalabad, 38090, Pakistan*
[b] *Department of Mechanics of Materials and Structures, Faculty of Civil and Environmental Engineering, Gdańsk University of Technology, Narutowicza 11/12, 80-233, Gdańsk, Poland*
[c] *formerly, School of Civil, Mining, and Environmental Engineering, University of Wollongong, NSW, 2522, Australia*

ARTICLE INFO

ABSTRACT

This study presents a modified crumb rubber (MCR) concrete design mix reinforced with multi-walled carbon nanotubes (MWCNTs), mechanical characterization, and cracking monitoring using the acoustic emission (AE) technique. The results showed that the bridging effect of MWCNTs and MCR in the concrete mix mitigated the shortcomings of MWCNT-MCR concrete and improved the flexural and compressive strengths by 18.3% and 26.5%, respectively, at 28 days. The stress-strain behavior of the MWCNT-MCR concrete showed improved ductility (48.12%), axial strain (50.12%), and toughness (27.15%) compared to the reference specimens. The MWCNT–MCR concrete exhibited a mechanical response in three distinct loading phases. Overall, tensile failure (>4000 μs/v and >35 kHz) was observed in the tested specimens through the RA value (ratio of rise time to amplitude of AE waves) and average frequency (AF) distribution. Based on the amplitude distribution of the AE waves, the damping capacity of the MWCNT-MCR concrete was improved by 27.83%, and the fracture mechanism between micro and macro cracks was identified through a b-value approach. Finally, a regression model was established to predict the E_c of MWCNT-MCR concrete and the two-way interaction effect on the mechanical properties of the developed mix design.

1. Introduction and background

Disposal of waste rubber tires is a serious concern for solid waste management authorities across the world which not only leads to drastic degradation of the built environment but also poses a fire hazard in stockpiling [1]. Burning of waste tires through inappropriate open fire or disposal in landfills near public places such as roadsides, commercial and residential areas, and valleys poses a high risk to human and animal health and the environment [2,3]. The annual production of waste tires is approximately 8.2 million tones corresponding to a total of 1.6 billion rubber production per annum across the world, with 60% of waste tires being disposed of through unknown or illegal means [4,5]. However, the utilization of crumb rubber in concrete is a way forward for a circular economy with promising benefits in terms of lowering environmental hazards and improving the overall mechanical performance of concrete [6,7].

In the last two decades, extensive research has been conducted to investigate the potential applications of waste rubber tires in concrete and asphalt pavements [8–10]. However, recent studies [11,12] reported that the mechanical strengths, such as the compressive and flexural strengths of the concrete mix, significantly decreased with the addition of crumb rubber. Such degradation in the mechanical properties of crumb rubber concrete is owing to the shape and particle size distribution of waste rubber tires [13]. In addition, poor interfacial bonding between the binding materials and recycled waste rubber was found to be a significant factor behind the decrease in the mechanical characteristics of crumb rubber concrete, as determined by Chen et al. [14] using scanning electron microscopy (SEM). Despite of the above limitations, the addition of crumb rubber in concrete improves the damping ratio and energy dissipation capacity [15,16], ductility, toughness, and impact/shock resistance [17], wear and frost resistance [18–20], with excellent crack controlling features in concrete. On the other hand, the recent advancements in nanotechnology led to the development of numerous micro-reinforcing structural materials that can be used for strengthening the matrix of the concrete. Carbon nanotubes (CNTs) and graphene nanoplatelets (GNPs) are promising nanomaterials for enhancing the mechanical characteristics of crumb rubber concrete [21,22]. Based on SEM, CNTs have a good structural and bond arrangement with excellent mechanical characteristics such as a high modulus ($E_c = 1$ TPa), high surface area, high tensile strength (100–150 GPa), and thermal and electrical conductivity with comparatively low weight compared to copper [23–25].

The effective utilization of nanostructured materials such as CNTs and GNPs in concrete mixes controls the microcracking pattern and improves the mechanical performance of hybrid CNT/GNP cement composites, such as fracture behaviour, ductility, and delayed eventual failure [26]. However, owing to their strong molecular bonds, the dispersion of nanomaterials such as CNTs and GNPs has always been challenging. Lin et al. [27] suggested mechanical stirring along with ultrasound treatment using organic surfactants to achieve a higher dispersion rate of nanomaterials in concrete mixes. J. Shao et al. [28] investigated the effect of CNTs and waste rubber tires on the mechanical performance of concrete. The study found that the compressive and flexural strengths improved by 19.73% and 10.14%, corresponding to the addition of 5% and 15% rubber in the concrete, respectively. Furthermore, Hao et al. [29] investigated the spalling of concrete prepared with different CNT contents and found that the probability of spalling of concrete was reduced by 20%, where CNTs acted as a crack propagation-resistant nanomaterial.

On the other hand, limited research studies have been carried out on the fracture evaluation and effective utilization of nanomaterials with a combination of industrial by-products in concrete, such as CNTs and modified crumb rubber (MCR). The fracture mechanism of concrete structures has always been a major concern owing to the brittle nature of concrete, which directly affects the structural safety, stability, and structural integrity of concrete structures under long-term performance [30]. Thus, an extensive investigation of nondestructive structural evaluation has been conducted on concrete structures to monitor the cracking pattern and fracture mechanism [31–34]. Among non-destructive evaluation (NDE) methods, acoustic emission (AE) is a well-known smart structural assessment technique that can be used to analyze the fracture mechanism and microcracking activities in concrete structures through the characterization of AE parameters [35–37]. The damping capacity, deterioration, damage recognition in concrete, crack propagation, and corrosion rate in steel structures can be precisely monitored through the characterization of AE parameters [38,39]. The classification of shear and tensile failures using the AE frequency distribution (AF) which is the total number of AE counts over time and rise time over the amplitude of AE signals (RA) in concrete structures, can be measured [40,41]. Concrete structures that undergo shear failure in compression will have shear cracks corresponding to lower AF and possess higher RA values, whereas others will have tensile cracks in bending corresponding to higher AF and relatively lower RA values [42,43]. Furthermore, extensive research has been conducted on the microstructural behaviour of recycled concrete structures against applied loading to understand the friction forces between two cracked surfaces, crack bridging, crack growth, and nucleation of shear and tensile cracks [44]. In addition, b-value analysis has been extensively used for the classification of micro- and macrocracks in concrete structures and cement composites [45,46]. Shiotani et al. [47] first developed improved b-value (Ib) model for progressive collapse in concrete structures using AE source. To differentiate between micro- and macro-cracks in concrete, Kurz et al. [48] reported that a decrease in the b-value can recognize the transfer of microcracks into macro-cracks through attenuation of AE signals during the fracture mechanism of concrete subjected to stress distribution. Carpinteri et al. [49] reported a b-value of 1.5 for the critical stage and cracks growth of concrete structures, while a b-value of 1.0 was recommended for the collapsed stage of concrete structures. Burud et al. [50] developed a generalized logistic model for b-value analysis to investigate the fracture process and validate it with the growth of micro- and macrocracking in plain concrete beams. Thus, the AE technique significantly improves damage detection in concrete structures using a multi-channel high-speed AE^{win} computational setup [51].

The recent advancement in the sustainable development of concrete structures has brought significant improvements in discovering the structural applications and strengthening of concrete because of the effective utilization of natural, engineered, and fiber wastes which can act as concrete substitutes [52,53]. A new eco-friendly concrete made from ground granulated blast slag (GGBS) and jute fibres (JF) was developed by Gulzar et al. [54]. The results showed considerable improvements in their mechanical properties. In addition, the permeability, mechanical characteristics, and life cycle assessment of high-strength concrete made from nylon waste fibres and micro-silica were studied which showed sound ductile behaviour and reduction of carbon footprint per unit concrete strength [55].

2. Research objectives

Despite the latest research on the mechanical properties, microstructural arrangement, fracture evaluation, and combined effect of industrial waste products (waste tire rubber) and nanomaterials such as CNTs on concrete structures, limited attention has been paid to the novel application of composite MWCNTs and MCR as reinforcing alternative and recycled industrial waste products in the construction of concrete structures. Therefore, keeping the potential scope of the cited construction materials and their monitoring

approach in mind, the current study demonstrates the following:

1. An innovative approach to modify and reduce the hydrophobic interactions of MCR using magnetic stirring.
2. Composite structural application of the MWCNT–MCR mix design in concrete and semi-rigid pavement.
3. A state-of-the-art solution to monitor and identify the combined fracture evaluation of the newly developed MWCNT–MCR concrete under mechanical loading through AE analysis.
4. The predictive model of E_c for determination of mechanical properties of MWCNTs-MCRC concrete.

3. Experimental and research program

3.1. Materials and mix proportions

In this study, an ordinary Portland cement (OPC) concrete of 30 MPa produced using cement, sand, and coarse aggregate with 0.43 w/c ratio as per ACI-211 [56] with different formulations of MWCNTs and MCR were used. Following the previous research studies [57,58], 0.4% and 0.8 wt% of CNTs content was replaced with cement by equal weight method. The particle size distribution of sand and waste tires rubber was carried out using sieve analysis as shown in Fig. 1(a). The mixes were prepared against 0%, 6%, and 12% of crumb rubber (size 1.5 to 2.5 mm in diameter and a density of 1070 kg/m^3 replaced with sand 1600 kg/m^3) by equivalent volume method. On the other hand, the coarse aggregate of size ranging from 9 mm to 21 mm with a density of 2644 kg/m3 were used without any replacement. A chemical solution called "Octyl-phenol-ethoxylate" was used as a surfactant for the dispersion of MWCNTs to achieve strong bonding. Table 1 shows the mix design and proportioning of MWCNTs-MCR. In this study, the micro-structural arrangement of MWCNTs in terms of C–H–S gel formation and role of MWCNTs in cracks bridging was studied using field emission scanning electron microscopy (FESEM) as showed in Fig. 1 (b). The detailed physical properties of MWCNTs and OPC are presented in Tables 2 and3).

3.2. Preparation of MWCNTs-MCR

Fig. 2 shows a detailed preparation and casting mechanism of hybrid MWCNTs-MCR. The bonding of MCR with the fine sand in mix and dispersion of MWCNTs in solution were the main challenges. Therefore, an electromagnetic field charges were used to enhance the bonding capacity of treated MCR, and electromagnetic stirrers were employed to perform dispersion and sonication of MWCNTs using a dispersion surfactant Octyl-phenol-ethoxylate to avoid cluster formation. At first stage, the amount of MWCNTs and surfactant with a ratio of 1:1 was introduced and mixed with a clean water free from impurities and salts. The suspension was mechanically stirred for 12 min and put into prob sonication assembly inside the vessel of cold water to avoid overheating and bond leakage of MWCNTs, followed by stirring at the speed of 3200 rpm for 25 min to get homogeneous dispersed solution.

The treated suspension of MWCNTs along with Portland cement, fine and coarse aggregate, and MCR were gently mixed in electrical multispeed planetary mixer with a speed ranging 300–400 rpm in a successive manner for 7 min. After mixing, the fresh MWCNTs-MCR mix were poured into a fabricated wooden and steel molds ($L \times W \times H = 500 \times 100 \times 100$) mm and ($D \times H = 150 \times 300$) mm in three layers, and each layer were compacted adequately to release the air voids. The specimens were demolded after 24 h, labeled, and cured at the room temperature (25 ^{0}C).

3.3. Testing setup

To determine the compression and flexural strengths of MWCNTs-MCR, hybrid testing setup (load + displacement control) was adopted. A Universal Testing Machine (UTM) with a capacity of 5000 kN and AE real time monitoring protocol was employed. Fig. 3 shows the experimental test setup used in this study. Two linear variable differential transducers (LVDT) and extensometers were attached on the specimens to determine the axial displacement and axial strain values, respectively. In addition, during the compression test, three electronic extensometers were attached at the mid height of the MWCNTs-MCR concrete cylinders in equal circumference distance. Two electronic extensometers were attached at the mid-span of MWCNTs-MCR prisms to get the stress-strain and load-deformation values of the tested MWCNTs-MCR specimens. The compression test on the cylindrical specimens was conducted under the load control protocol. However, a hybrid control mechanism was adopted for three-point bending test.
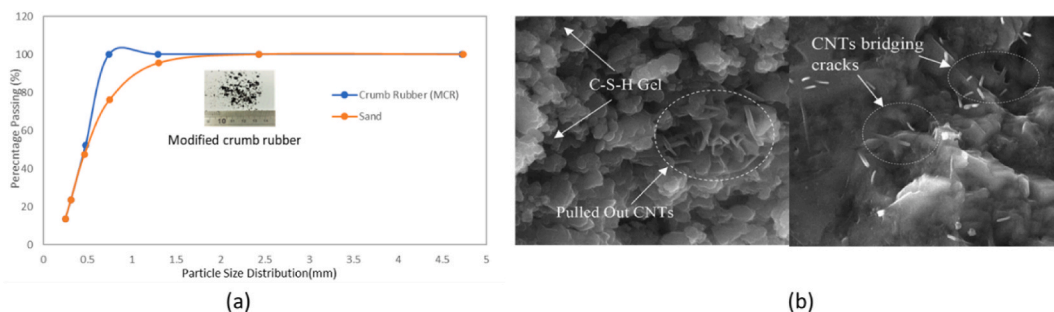

Fig. 1. (a)Sieve analysis of fine aggregates; and (b) microstructural arrangement of MWCNTs.

Table 1
Mix design and proportioning of MWCNTs-MCRC.

Mix ID	w/c	Crumb rubber (%)	MWCNTs (% wt.)	Surfactant	Water (Kg/m³)	Fine aggregate (Kg/m³)	Coarse aggregate (Kg/m³)	Cement (Kg/m³)	Crumb rubber (Kg/m³)
R0CNT0	0.43	0	0	1:1	199	732	944	458	0
R6CNT0.4	0.43	6	0.4	1:1	199	713	944	457	4.40
R12CNT0.4	0.43	12	0.4	1:1	199	689	944	457	8.80
R6CNT0.8	0.43	6	0.8	1:1	199	713	944	457	4.40
R12CNT0.8	0.43	12	0.8	1:1	199	689	944	457	8.80
MCR6	0.43	6	0	0	199	713	944	458	4.40
MCR12	0.43	12	0	0	199	689	944	458	8.80

Table:2
Physical properties of multi-walled carbon nanotubes (MWCNTs).

Diameter	Specific surface area	Length	Purity	Electric conductivity	Bulk density
(mm)	(m²/g)	(μm)	(%)	(s/cm)	(g/cm3)
20–30	>110	10–30	>98	>100	0.29

Table 3
Physical properties of P.0 42.5 reference cement.

Density (g/cm³)	Specific Surface Area(m²/kg)	Consistency (%)	Setting Time (min)		Compressive Strength (MPa)		Flexural Strength (MPa)	
			Initial Sitting	Final Sitting	3d	28d	3d	28d
3.2	355	28	161	240	33.0	57.2	6	8.2
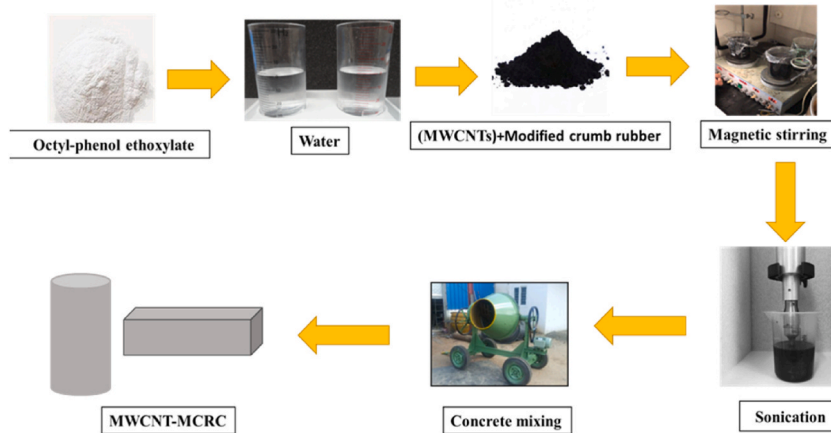
Fig. 2. Preparation of MWCNTs-MCR.

3.3.1. AE monitoring and b-value analysis

In this study, a smart structural health monitoring setup comprised of PC AE^{win} sensor-based acoustic multi-channel operating system (SAMOS) with typical AE characteristics was used. The setup comprised of four high resonant AE sensors, two R6α and two R15α having a frequency range of 35–150 kHz and 50–500 kHz, respectively. AE preamplifier was used to enhance the strength of AE signals with a nominal range between 20 and 50 dB. Digital type 2/4/6, MISTRAS Group, and AE data training devices named PCI-2 board were employed to monitor the micro-cracking and fracture behavior of MWCNTs-MCR specimens. A threshold limit of 50 dB was set to avoid the effect of noise during cracking and occurrence of AE counts. In addition, a sampling frequency of 10 MHz along with the band-pass filter between 10 kHz and 2 MHz was set to record AE activities. The specimens were tested using the loading rate of 0.25 MPa/s and 0.5 mm/min under compression and three-point bending, respectively. AE sensors (two R6α and two R15α) were attached at the regular intervals to get the AE activities data as shown in Fig. 3(a). Thus, the entire PC AE^{win} system correlated AE activities corresponding to growth rates and cracking behavior of specimens during testing. Only the micro-cracking monitoring results of four different AE parameters as presented in section 3.3 obtained from the compression test of specimens were analyzed to check the feasibility of acoustic emission analysis for the structural assessment of MWCNTs-MCR.

It is noted that a precise observation is required to monitor the complex inter-molecular bonding and micro-cracking activities in
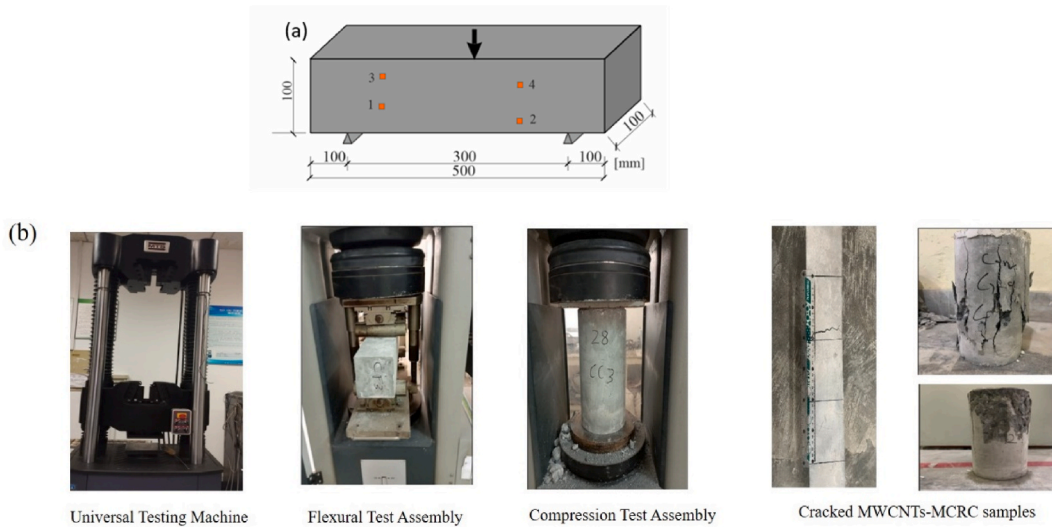
Fig. 3. Schematic representations of (a)AE sensor position and (b)experimental testing program.

MWCNTs along with MCR content in concrete matrix. Therefore, AE technique along with b-value analysis was adopted to monitor the fracture mechanism of hybrid concrete matrix. Fig. 4 shows AE parameters such as amplitude (peak voltage in decibels) and frequency (rate of change of AE hits) distribution, rise time (duration between peak voltage and first threshold crossing), and total duration (D), respectively. AE counts are the time difference between last and first threshold crossing of total number of activities that cross the threshold limit during fracture process.

4. Results and discussions

4.1. Dispersion rate of MWCNTs

Ultraviolet (UV) spectrometry and Beer-Lambert law was carried out to determine the strength and concentration, and water absorption of MWCNTs with 20-min, 40-min, and 60-min manual sonication's, respectively. Lambert-Beer's law suggested Equation (1) for the absorption rate of MWCNTs-MCR.

$$A = log \frac{1}{T} = log \frac{I_r}{I_s} = ECl$$ Eq. (1)

where A = absorbance, T = light transmittance, Ir = intensity of incident radiation, Is = intensity of transmitted radiation, E = molar absorption coefficient, c = solution concentration and l = optical path length.

It is noted that, there is a linear relationship between the strength and water absorption capacity of MWCNTs dispersed solution in certain range of wavelength during first 1-hr sonication. There was a consistent increase observed in the absorbance rate of 0.4% and 0.8 wt% MWCNTs aqueous solution against 20-min- and 40-min sonication's. However, a promising response was shown by R6CNT0.4 concrete mix in both 20 and 40-min sonication's in terms of better absorbance rate than that of 0.8 wt% MWCNTs which is 6.8% and 8.3%, respectively. Based on the dispersion test results (as showed in Table 4), a 40-min sonication was recommended for the dispersion of different wt.% MWCNTs, as there was no significant improvement found after the sonication time extended from 40 to
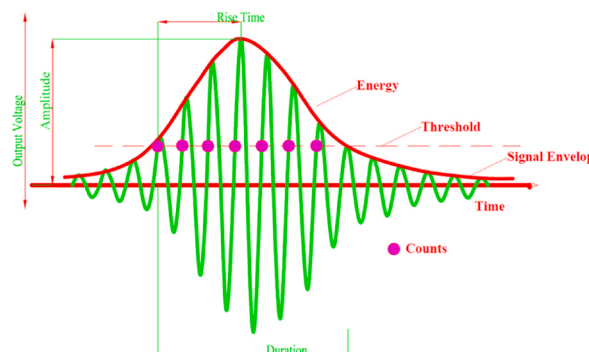

Fig. 4. Typical AE evaluation parameters.

60-min due to cluster formation and bond leakage between the nanoparticles.

4.2. Mechanical characterization

Fig. 5 shows the comparison between pure crumb rubber and the applications of MWCNTs concrete in terms of average stress-strain behavior under axial compressive loading at 28 days. As depicted in Fig. 5(a), the MWCNTs-MCR specimens tested under compression loading, exhibited three distinct mechanical phases that were not evident in the reference specimens. The three mechanical phases observed in all tested MWCNTs-MCR specimens were: (I) pre-peak phase, (II) transition phase, and (III) post-peak phase. The MWCNTs-MCR specimens showed higher micro-cracking activities followed by a gradual decrease in compression strength. Such variation in the stress-strain response of tested specimens was attributed to addition of different wt.% of MWCNTs and MCR. Further, a similar conclusion was derived from the pure crumb rubber concrete with addition of 6% and 12% modified crumb rubber. On the other hand, the response of reference specimens was entirely brittle with less micro-cracking activities followed by an abrupt decline in compression capacity. As showed in Fig. 5(b), the axial strain, ductility, and toughness of specimen MCR6 was improved by 50.10%, 48.12%, and 27.15%, respectively compared to R0CNT0.

As presented in section 3.3.2, MWCNTs-MCR specimens exhibited higher Ec in phase (I) and improved by 31.19% compared to MCR specimens. MWCNTs-MCR specimens showed higher toughness as well as long tail deformation during phase (II) and phase (III) against the compressive loading. The incorporation of MWCNTs in rubberized concrete can mitigate the shortcomings (compressive and flexural strengths) pertaining to excellent dispersion of MWCNTs and treatment of MCR. The specimens with 0.4 wt% MWCNTs and 6% MCR exhibited highest flexural strength (5.03 MPa) and compressive strength (43.32 MPa) compared to that of with 0.8 wt% MWCNTs.

4.2.1. Compressive and flexural and strengths of MWCNTs-MCR

Fig. 6 shows the compressive and flexural strengths of MWCNTs-MCR specimens with different wt.% of MWCNTs and MCR tested at 7, 14 and 28 days. As depicted in Fig. 6(a), the compressive strength was increased by 17.60%, 27.38% and 26.51% at 7, 14, and 28 days, respectively with the addition of 0.4% MWCNTs + 6% MCR in the mix compared to the reference specimens. In addition, their flexural strength was increased by 12.67%, 19.11% and 18.29% at 7, 14, and 28 days with the addition of 0.4% MWCNTs +6% MCR, respectively compared to the reference specimens. Such improvement in mechanical properties of MWCNTs-MCR concrete mix was due the homogeneous dispersion of MWCTs achieved with 40-min sonication and development of two-dimensional sp^2 - sp^2 dense packed hybridized structure of MWCNTs. Thus, it is evident that inclusion of MWCNTs in concrete has the potential to increase the compressive and flexural strengths of concrete compared to the simple addition of MCR as partial replacement of sand in concrete matrix. However, Fig. 6(b) shows that there was no such improvement observed to enhance the mechanical performance of MWCNTs-MCR matrix with the addition of 0.8 wt% MWCNTs contents due to massive cluster formation except a post-peak ductile response against the compressive loading.

4.2.2. Elastic modulus (Ec) of MWCNTs-MCR

The static modulus of elasticity (Ec) of MWCNTs-MCR cylindrical specimens tested at 28 days was evaluated using ASTM C496 [59]. As shown in Table 5, the reference specimen (R0CNT0) exhibited the maximum (Ec) compared with the concrete matrix containing different wt. % of MWCNTs and MCR. However, the (Ec) of R6CNT0.4 and R12CNTs0.4 was improved by 22.77% and 27.02%, respectively, with the addition of 0.4 wt % of MWCNTs in concrete specimens compared to the simple addition of modified crumb rubber in MCR6 and MCR12 matrixes. A concrete matrix containing 0.4% MWCNTs and 6% MCR achieved the maximum (Ec) (29.77 GPa) among all the concrete mixes, except for the reference specimen. In contrast, the concrete matrix containing 0% MWCNTs and 12% MCR (MCR12) exhibited the lowest (Ec) (21.12 GPa). It can be concluded that the addition of MWCNTs has a major influence on the compressive stress-strain behaviour of MWCNT-MCR which directly affects (Ec). Therefore, the (Ec) of MWCNTs-MCR can be further optimized through the inclusion of varying wt. % of MWCNTs and MCR.

4.2.3. Ductility

The ductility factor μ_φ was calculated from the stress-strain curves of MWCNTs-MCR specimens using Equation (2), as illustrated by Ali et al. [60]. As shown in Table 5, the specimens prepared with the incorporation of MWCNTs and MCR achieved the maximum ductility factor compared with the reference specimens. A total of 25% and 26% increases were found in the ductility of MCR6 and MCR12, respectively, compared to the reference specimens. Overall, this phenomenon indicates that the addition of nano-modified materials and MCR in the concrete mix results in higher ductility during post-peak behaviour under compression loading.

Table 4
Dispersion level of MWCNTs-MCRC.

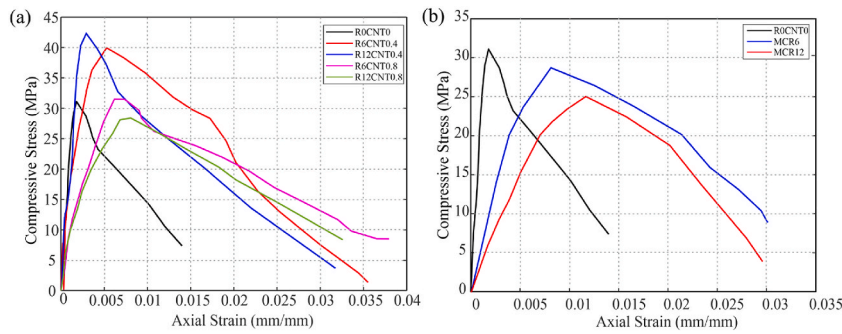| Specimens ID	Handshake Absorbance (%)	20-min Absorbance (%)	40 min Absorbance	60-min Absorbance (%)
R6CNT0.4	3.5	6.8	8.3	6.5
R12CNT0.4	3.4	5.9	8.2	7.6
R6CNT0.8	3.6	6.0	7.9	7.1
R12CNT0.8	3.3	5.70	7.5	6.80
MCR6	2.7	3.6	4.1	3.8
MCR12	2.2	3.40	3.8	3.7

Fig. 5. Stress-strain behavior of cylindrical specimens; (a) 6% and 12% crumb rubber with 0.4% and 0.08% of CNTs; (b) 0%, 6%, and 12% crumb rubber with 0% of CNTs.
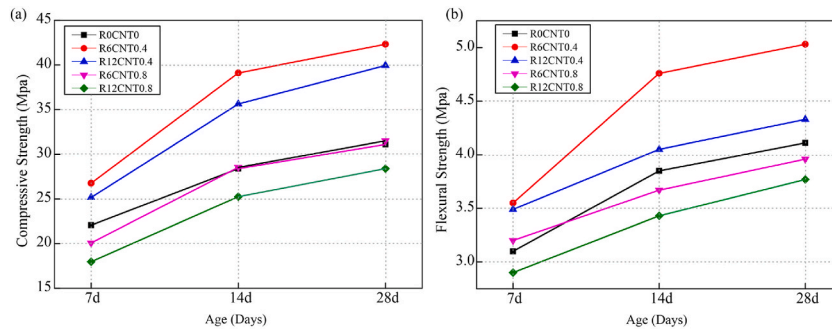

Fig. 6. Mechanical strengths of MWCNTs-MCR; (a) compressive strength; (b) flexural strength.

Table 5
Mechanical strengths of MWCNTs-MCRC.

Mix ID	Flexural Strength (MPa)	Compressive Strength (MPa)	Modulus of Elasticity *(Ec)* (GPa)	**SD**(*fc*)	**SD**(*ft*)	**SD**(*Ec*)	Ductility (μ$_\Phi$)
R0CNT0	4.11	31.1	29.77	5.92	0.61	3.27	1.59
R6CNT0.4	5.03	42.32	29.5				2.12
R12CNT0.4	4.33	39.94	28.94				2.47
R6CNT0.8	3.96	31.5	25.22				1.89
R12CNT0.8	3.77	28.4	23.69				2.25
MCR6	3.42	28.12	22.77				2.75
MCR12	2.95	25.07	21.12				2.96

Note: *SD* is standard deviation; *fc* is compressive strength; *ft* is flexural strength; and *Ec* is elastic modulus.

$$\mu_\varphi = \frac{\Delta\epsilon_1}{\Delta\epsilon_2}$$

Eq. (2a)

Where $\Delta\epsilon_1$ is the strain corresponding to the horizontal line intersected by tangent during pre-peak behaviour, while $\Delta\epsilon_2$ is the strain obtained against the 80% of the compressive strength during post-peak behaviour.

4.3. Acoustic emission (AE) analysis

4.3.1. Cumulative AE hits activities of MWCNTs-MCR

The dataset obtained from the compression test of the cylindrical specimens was used to evaluate the cracking pattern and fracture mechanism of MWCNTs-MCR. As illustrated in Fig. 7, the variation among AE activities corresponding to the load and time duration was monitored in the tested specimens in three different phases (I), (II), and (III). It was observed that the load–time and cumulative AE events gradually increased with a steep slope in all specimens during the pre-peak phase (I). This phenomenon indicates that the maximum number of microcracking activities with multiple cracking patterns was traced by the AE sensors mounted on the specimens. As revealed by the curve trend of cumulative AE events, the microcracking activities were also found to increase, which was further followed by a gradual decrease in the compressive strength in phase (II). A flat slope of cumulative AE activities in Phase (III) was obtained which indicates that the specimens had reached the collapse stage; thus, no further microcracking activities were recorded by the AE sensors. This was due to the addition of MCR into the concrete mix which arrested the major cracking pattern and improved the
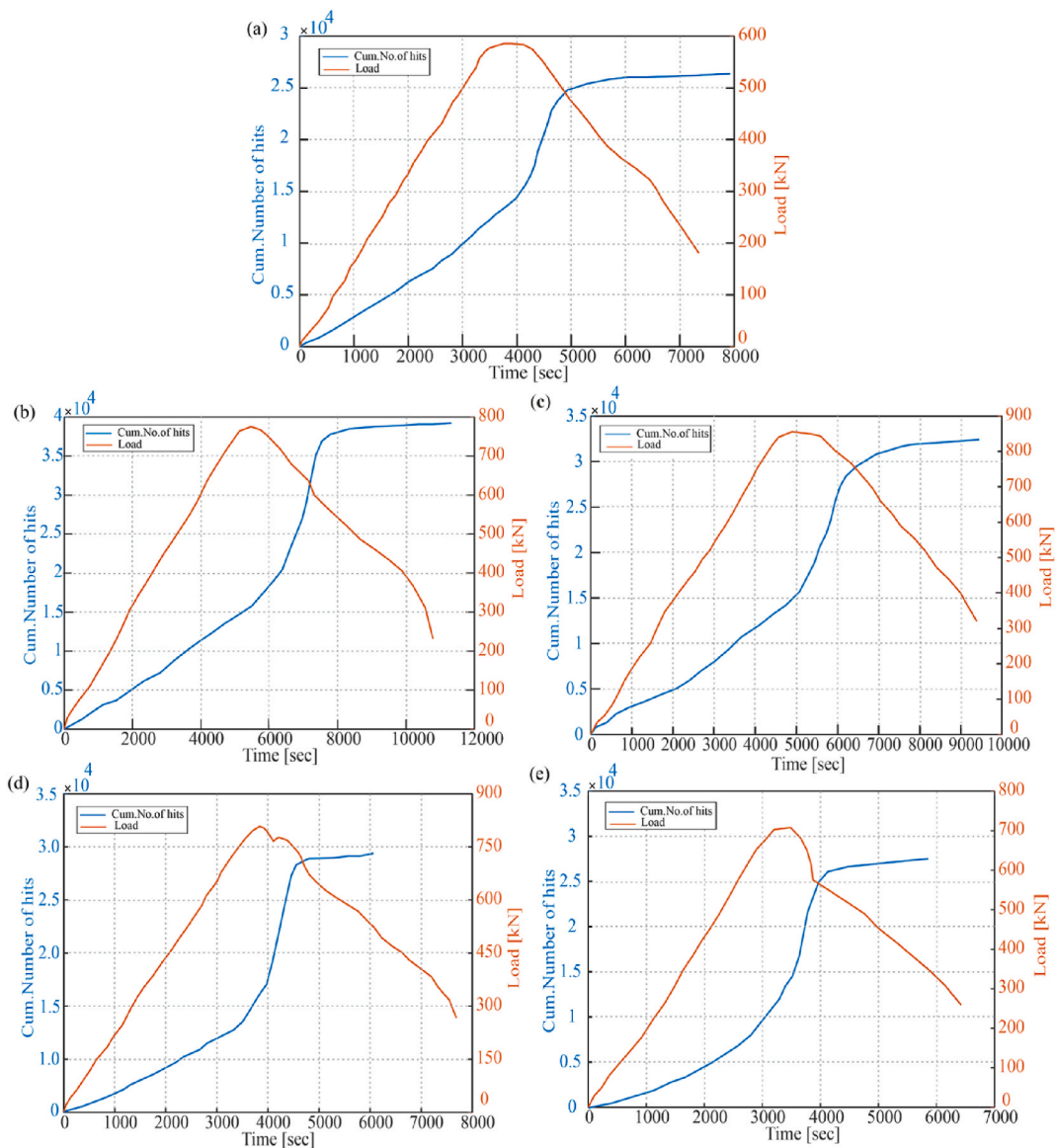
Fig. 7. Cumulative AE hits and load-time curves of MWCNTS-MCR: (a) MCR = 0%, MWCNTs = 0%; (b) MCR = 6%, MWCNTs = 0.4%; (c) MCR = 12%, MWCNTs = 0.4%; (d) MCR = 6%, MWCNTs = 0.8%; (e) MCR = 12%, MWCNTs = 0.8%.

post-peak behaviour of MWCNTs-MCR specimens.

Furthermore, a significant variation in terms of cumulative AE events and time duration corresponding to compression loading between the reference and MWCNT–MCR specimens was found, as shown in Fig. 7(b–e). The incorporation of different MWCNTs contents (wt. % and MCR resulted in higher AE events in modified concrete mix compared to reference sample. The sample R12CNT0.4 showed the highest AE events (3.8×10^4) and time duration (10.47×10^3 s) among all tested specimens. On the other hand, the calculated AE events and time duration of the reference specimens against the applied loading were found to be 2.25×10^4 and 7.3×10^3 s, respectively. This is because MWCNTs-MCR matrix has excellent resistance and bonding strength against compressive loading which results in higher AE events and longer time duration compared to the reference specimens.

4.3.2. Fracture mechanism of MWCNTs-MCR based on RA vs. AF analysis

Fig. 8 depicts the damage classifications (shear and tensile) of MWCNTs-MCR matrix through two different fracture precursors, RA and AF [61]. Gong et al. [62] reported that irrespective of the type of AE sensor, lower RA values (<4000 μs/v) followed tensile fracture activities, whereas higher RA values (>4000 μs/v) indicated shear failure during AE monitoring of the specimens. As evident from the literature [63,64], a lower AF value (>35 kHz) of the specimens showed shear failure, whereas a higher AF value (<35 kHz) resulted in tensile failure. Fig. 8(a) shows a higher RA value in phase (I) with abrupt crack initiations in terms of scattered AE events; however, a significant increase in the RA value can be observed during phases (II) and (III). In addition, an increment in the AF value
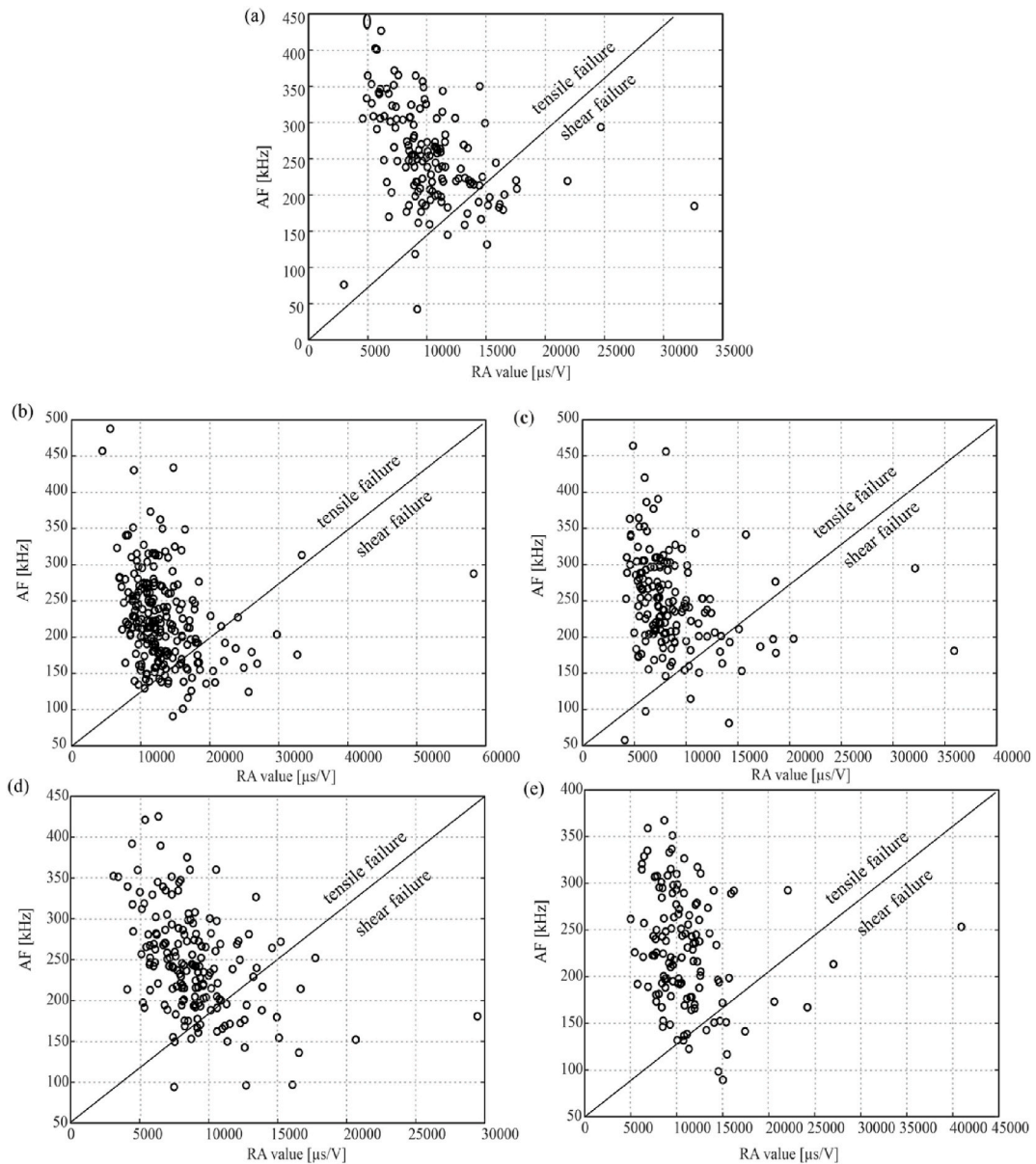
Fig. 8. RA value and frequency distribution of MWCNTS-MCR: (a) MCR = 0%, MWCNTs = 0%; (b) MCR = 6%, MWCNTs = 0.4%; (c) MCR = 12%, MWCNTs = 0.4%; (d) MCR = 6%, MWCNTs = 0.8%; (e) MCR = 12%, MWCNTs = 0.8%.

from 65 kHz to 350 kHz in phase (I) to phase (III) during the entire microcracking monitoring of the MWCNT-MCR specimens was observed. Based on the obtained results, MWCNTs-MCR specimens (see Fig. 8(b–e)) showed tensile failure with maximum clustered AE events compared to the reference specimen which exhibited tensile failure. Thus, it was concluded that the inclusion of MWCNTs and MCR in plain concrete can evidently shift the failure pattern and classify the fracture mechanism through RA-AF parameters between various modes.

4.3.3. Amplitude distribution characteristics of MWCNTs-MCR

Fig. 9 shows the damping response of the tested specimens through the amplitude distribution of the AE waves under different loading configurations. MCR (0–12%) and MWCNTs (0–0.8%) were found to be the main factors influencing the amplitude distribution of AE. The loading time of MWCNTs-MCR specimens increased with the addition of MCR which resulted in a significant variation in the damping ratio in all the loading phases compared to the reference specimen. During AE monitoring (see Fig. 9(a)), an amplitude distribution ranging from to 40–70 dB of AE waves corresponding to $0\text{-}5 \times 10^3$ s with a smaller number of AE events under the load curve in the reference specimens was recorded. However, as demonstrated in Fig. 9(b–e), this range of amplitude distributions of AE events in MWCNTs-MCR specimens was found to be 0–80 dB corresponding to $0\text{-}10 \times 10^3$ s, with a higher number of AE events under
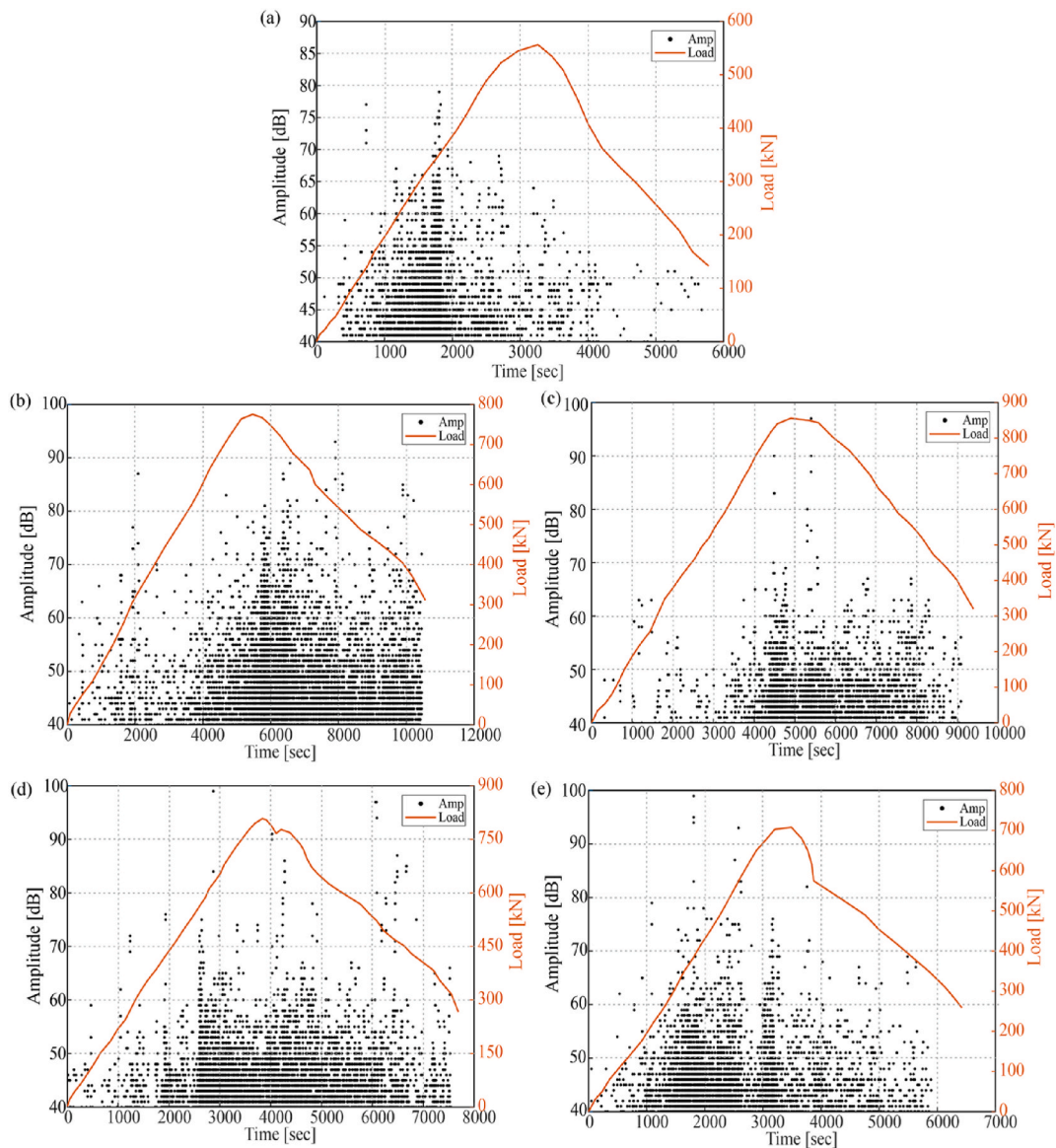
Fig. 9. Amplitude of distribution of MWCNTS-MCR: (a) MCR = 0%, MWCNTs = 0%; (b) MCR = 6%, MWCNTs = 0.4%; (c) MCR = 12%, MWCNTs = 0.4%; (d) MCR = 6%, MWCNTs = 0.8%; (e) MCR = 12%, MWCNTs = 0.8%.

the load curve. On average, the damping capacity of MWCNTs-MCR specimens increased by 27.83% compared to that of the reference specimen. These arguments indicate that the shock absorption and damping capacity of concrete can be significantly improved by adding a suitable proportion of MWCNTs and MCR.

4.3.4. b-value approach

The b-value ND evaluation was adopted particularly to analyze micro-, and macro-cracks of hybrid concrete matrix. Gutenberg et al. [65] first proposed the linear empirical model of b-value analysis through the given Equation (2).

$$\log_{10} N\,(M) = a - bM \qquad\qquad \text{Eq. (2b)}$$

Where $N(M)$ represents total number of AE activities with varying amplitude under real monitoring time; and a, b are two linear AE empirical constants. Based on the literature [66], the structural members with higher AE activities and less AE amplitude detect microcracks, while those having less AE activities and higher AE amplitude detect macro-cracks. Therefore, equation (1) was further simplified using acoustic emission energy AE and amplitude distribution and is given as Equation (3).

$$\log_{10} N = a - b' \left(\frac{A_{dB}}{20} \right) \qquad \text{Eq. (3)}$$

where (N) is the likelihood AE events during microcracking activities, b' is the slope of line corresponding to cracking to the cracking; and A_{dB} is the amplitude of peak voltage in terms of decibels.

It is noted that a concrete structure with a higher b-value during the fracture mechanism represents microcracks, whereas a lower b-value indicates macrocracks. In this study, MATLAB was used to analyze and classify the recorded fractured b-value data of the reference and MWCNT-MCRC specimens from the compression test only. As illustrated in Fig. 10, an evident variation in the b-value is observed in the concrete matrix corresponding to the compression load. Multiple micro-cracking activities with an average b-value of 1.89 was detected in the initial phase (I) in all specimens which resulted in higher AE energy released during micro-cracking with less fracture magnitude under compressive loading. However, as shown in Fig. 10(b–e), the MWCNT-MCR specimens exhibited a higher number of AE activities with an average b-value of 2.9 during the ultimate load-carrying time. It is further illustrated that MWCNTs-MCR specimens showed the maximum number of peaks compared to the reference specimen under peak loading for a longer period. This unique characteristic indicates that the addition of MWCNTs and MCR increases the sensitivity and intermolecular bonds and delays the crack propagation of concrete under mechanical loading. In addition, the b-values gradually decreased after the peak load in phase (III), which resulted in the macro-cracking mechanism of the tested specimens. Thus, it was concluded that the b-value,

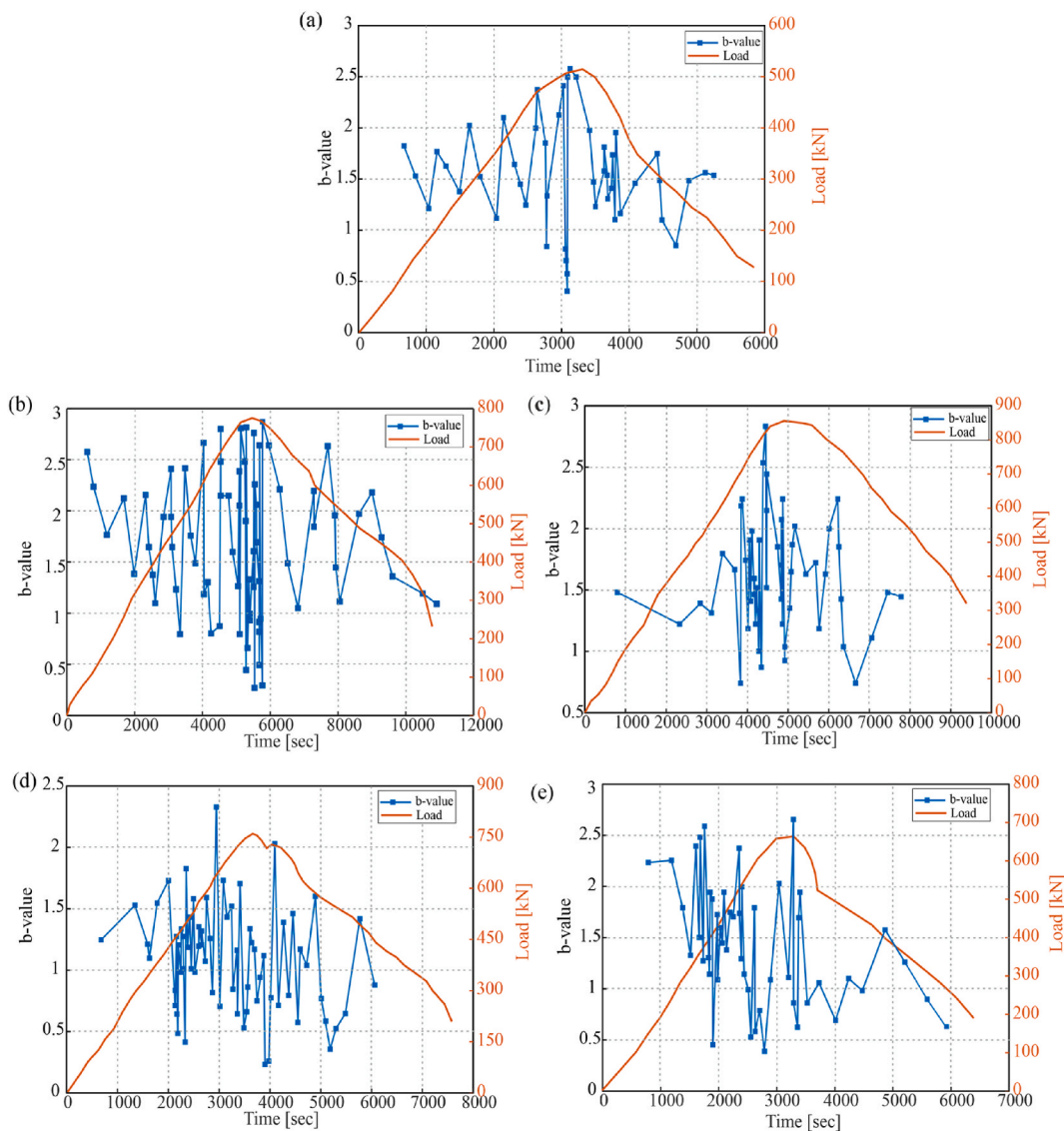**Fig. 10.** Cracking classifications of MWCNTS-MCR using b-value analysis: (a) MCR = 0%, MWCNTs = 0%; (b) MCR = 6%, MWCNTs = 0.4%; (c) MCR = 12%, MWCNTs = 0.4%; (d) MCR = 6%, MWCNTs = 0.8%; (e) MCR = 12%, MWCNTs = 0.8%.

including the time duration (N), can be chosen as a precursor to differentiate micro- and macro-cracking patterns in concrete structures before and after peak excitations.

4.4. Regression analysis of MWCNTs-MCR

A regression analysis was performed to predict the optimum compressive and flexural strengths of MWCNTs-MCR matrix using Minitab 18.1 software. Tables 6 and 7) present the impact of different independent variables (MWCNTs, MCR, and surfactant) and two-way interactions (MWCNTs-MCR, MWCNTs-surfactant, MCR-surfactant) on the dependent variables (compressive and flexural strengths) of the MWCNT-MCR specimens. The outcomes were analyzed based on F and P-vales tests of the trained dataset obtained from the stress-strain response of the specimens. The p-values of regression, MCR, and MWCNTs and two-way interactions of MWCNTs-MCR at the 95% confidence level were less than 0.05 which showed the most significant behaviour; however, the surfactant and its interaction with MCR and MWCNTs with a p-value greater than 0.05, showed an insignificant effect on the compressive and flexural strengths of MWCNTs-MCR. This can be explained by the fact that the compressive and flexural strengths can be greatly varied with the percentage addition of MWCNTs and MCR, while there was less effect of surfactant on the optimum prediction of mechanical performance of MWCNT-MCR. A similar observation was derived from the analysis of the F-test of MWCNTs-MCR.

4.4.1. Predictive model of Ec of MWCNTs-MCR

In this study, a model to predict the *Ec* of MWCNT-MCR was developed using a regression analysis of the compressive strength of cylindrical specimens. The compressive strength was considered as the governing mechanical parameter to establish the relationship with *Ec*, as shown in Fig. 11(a). The model *Ec* of MWCNT-MCR was optimized through factorial analysis using the following statistical parameters including F and P-value tests: (I) root-mean square error (RMSE) for the degree of scattered data set in terms of outliers; (II) R-square (R2) for the best-fitted line between actual and predicted results of MWCNT-MCR; and (III) mean-absolute percentage error (MAPE) for the total error between the measured and predicted values of *Ec* of MWCNT-MCR. The following regression-based model, as presented by Equation (5), was developed to predict the *Ec* of MWCNT–MCR.

$$Ec = 6.431 \times \sqrt{fc'} - 9.5 \qquad \text{Eq. (5)}$$

In addition, the developed model for *Ec* is compared and validated with various standards and existing models proposed in the literature. The predicted results obtained using the model developed in this study are consistent with those of EC [67], ACI-363 [68], ACI-318 [69], and CSA. A23.3 [70], Norway [71], Rashid et al. [72], and Jalal et al. [73] are listed in Table 8. Fig. 11(b) shows the validation and comparison of the results predicted using the developed model for Ec with those of different models adopted in the literature. The results show that the R^2 value of the proposed model is greater than 92%, along with the minimum mean absolute percentage error (MAPE), and can be effectively used to predict the *Ec* of MWCNT-MCR.

5. Conclusion

This study investigated the mechanical properties of MWCNT–MCR under the influence of MWCNTs and MCR using experimental AE evaluation and statistical methods. The flexural and compressive strengths, elastic modulus (Ec), dispersion rate of MWCNTs, and AE monitoring were investigated in detail to characterize the mechanical behaviour of the MWCNT-MCR. Based on the results, the following conclusions were drawn:

1. To achieve the optimum dispersion of the MWCNTs suspension, 40-min ultrasonic sonication time with an absorbance rate of 6.8%–8.3% was recommended in the presence of a surfactant (1:1). The optimum compressive strength 42.32 MPa and flexural strength 5.03 MPa were recorded at these dispersion rates.

2. The bridging effect of MWCNTs controlled the weak interfacial bonding between cement and MCR, which resulted in an improvement of 26.51% in compressive strength (f_c'), 18.29% in flexural strength (f_t), and 22.77% in elastic modulus (E_c) with the addition of 0.4 wt% MWCNTs and 6% MCR compared to the reference specimens.

3. Through AE evaluation, MWCNTs-MCR showed a steep slope with post-ductile stress-strain behaviour in three distinct phases under axial compression loading. Addition of different amounts of wt.% MWCNTs in concrete enhanced the axial strain and toughness by 50.10%, and 27.15%, respectively, due to strong Van der Waals bonding.

4. Using fracture analysis, tensile failure with dense clusters was observed in MWCNT-MCR specimens through precise monitoring of AE precursors (RA values and AF). In addition, the micro- and macro-cracks were effectively differentiated using an improved b-value approach with an average b-value of 2.9 during the ultimate load-carrying time.

5. Based on the amplitude distribution of the AE waves, the damping capacity and ductility of MWCNTs-MCR were improved by 27.83% and 26%, respectively, which can be attributed to the addition of MCR dosages in the concrete mix.

6. The two-way interaction of MWCNTs and MCR showed more significant behaviour in improving the mechanical properties of MWCNTs-MCR specimens.

7. A regression-based model developed in this study to predict E_c of MWCNTs-MCR showed reasonable agreement with the results in the literature for the prediction of E_c of MWCNTs-MCRC.

Finally, it can be concluded that the commercial use of MCR and MWCNTs in concrete mix can significantly improve the mechanical properties of concrete structures and cracking patterns, and meet the target of circular economy and the construction of sustainable infrastructure goals.

Table 6
Analysis of variance (compressive strength).

Source	DF	Adj SS	Adj MS	F-Value	P-Value
MCR	1	75.75	75.75	3.20	0.0041
MWCNTs	1	94.90	94.90	3.41	0.0014
Surfactant	1	49.90	49.90	1.57	0.0780
MWCNTs-MCR	1	96.22	96.22	3.59	0.0018
MWCNTs-Surfactant	1	79.45	79.45	2.96	0.0046
MCR-Surfactant	1	57.72	57.72	1.67	0.0322

Table 7
Analysis of variance (flexural strength).

Source	DF	Adj SS	Adj MS	F-Value	P-Value
MCR	1	73.45	73.45	2.92	0.0049
MWCNTs	1	92.93	92.93	3.77	0.0033
Surfactant	1	51.51	51.51	1.66	0.1280
MWCNTs-MCR	1	94.69	94.59	3.41	0.0020
MWCNTs-Surfactant	1	76.33	76.33	2.96	0.0055
MCR-Surfactant	1	49.54	49.54	1.67	0.0734
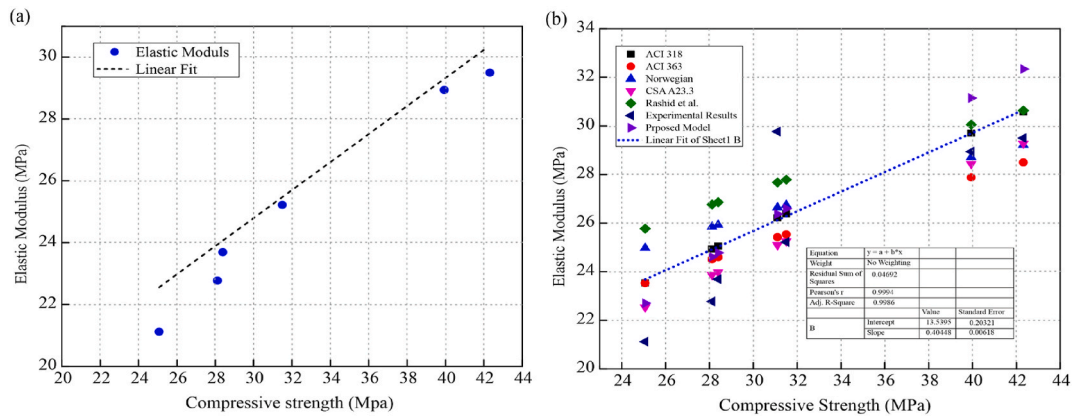
Fig. 11. Illustration of Ec of MWCNTs-MCR; (a) Comparison between compressive strength and *Ec*; (b) Comparison of proposed regression-based model with experimental and existing standards.

Table 8
Existing models for predictions of *Ec* proposed by different standards and scholars.

Reference	Existing Models	Limitations
ACI 318 [69]	$E_c = 4.7 \times \sqrt{f_c'}$	–
ACI 363 [68]	$E_c = 3.32 \times \sqrt{f_c'} + 6.9$	21 MPa $< f_c' <$ 83 MPa
CSA A23.3 [70]	$E_c = 4.5 \times \sqrt{f_c'}$	20 MPa $< f_c' <$ 40 MPa
Norwegian [71]	$E_c = 9.5 \times (f_c')^{0.3}$	25 MPa $< f_c' <$ 85 MPa
EC [67]	$E_c = 22 \times (0.1 f_c')^{0.3}$	–
Rashid et al. [72]	$E_c = 8.9 \times (f_c')^{0.33}$	20 MPa $< f_c' <$ 130 MPa
Jalal et al.(a) [73]	$E_c = 6.157 \times \sqrt{f_c'}$	10% rubber content
Jalal et al.(b) [73]	$E_c = 6.486 \times \sqrt{f_c'}$	15% rubber content

CRediT authorship contribution statement

Suliman Khan: Conceptualization, Methodology, Data curation, Visualization, Writing – original draft, Writing – review & editing. **Shahzad Ashraf:** Investigation, Resources, Visualization, Data curation, Software, Writing - review & editing. **Shehroze Ali:** Visualization, Formal analysis, Writing – review & editing. **Khushal Khan:** Formal analysis.

Declaration of competing interest

Authors declare no conflict of interest.

Data availability

Data will be made available on request.

References

[1] Ronald A. Bailey, Herbert M. Clark, James P. Ferris, Sonja Krause, L. Robert, Strong. 16 - Solid Waste Disposal and Recycling, Chem of the Envir, second ed., Academic Press, 2002, pp. 769–792, 9780120734610.

[2] Z.C. Steyn, A.J. Babafemi, H. Fataar, R. Combrinck, Concrete containing waste recycled glass, plastic and rubber as sand replacement, Construct. Build. Mater. (2021) 269.

[3] G.F. Cardamone, F. Ardolino, U. Arena, About the environmental sustainability of the European management of WEEE plastics, Waste Manage. (Tucson, Ariz.) 126 (2021) 119–132.

[4] M. Arabiourrutia, G. Lopez, M. Artetxe, J. Alvarez, J. Bilbao, M. Olazar, Waste Tyre Valorization by Catalytic Pyrolysis – A Review, vol. 129, Renewable Sustainable Energy Rev, 2020.

[5] K. Formela, Sustainable development of waste tires recycling technologies – recent advances, challenges, and future trends, Adv Ind Eng Polym Res 4 (3) (2021) 209–222.

[6] E. Ganjian, M. Khorami, A.A. Maghsoudi, Scrap-tyre-rubber replacement for aggregate and filler in concrete, Construct. Build. Mater. 23 (5) (2009) 1828–1836.

[7] V. Corinaldesi, Structural concrete prepared with coarse recycled concrete aggregate: from investigation to design, Adv. Civ. Eng. 2011 (2011).

[8] A.B. Awan, F.U.A. Shaikh, Structural behavior of recycled tire crumb rubber sandwich panel in flexural bending, Struct. Concr. 22 (6) (2021) 3602–3619.

[9] W. Zhang, Z. Zhang, Q. Zhao, Laboratory performance evaluation of a waterborne epoxy-modified asphalt mixture with styrene-butadiene rubber for cold patching applications, J. Mater. Civ. Eng. 34 (6) (2022).

[10] H.- Yu, G.- Deng, D.- Wang, Z.- Zhang, M. Oeser, Warm asphalt rubber: a sustainable way for waste tire rubber recycling, J Cent South Univ 27 (11) (2020) 3477–3498.

[11] J. Xu, Z. Fu, Q. Han, G. Lacidogna, A. Carpinteri, Micro-cracking monitoring, and fracture evaluation for crumb rubber concrete based on acoustic emission techniques, Struct. Health Monit. 17 (4) (2018) 946–958.

[12] J. Xu, Z. Fu, Q. Han, H. Li, Fracture monitoring and damage pattern recognition for carbon nanotube-crumb rubber mortar using acoustic emission techniques, J Struct Control Health Monit 26 (10) (2019).

[13] R. Kumar, N. Dev, Mechanical and microstructural properties of rubberized concrete after surface modification of waste tire rubber crumb, Arabian J. Sci. Eng. 47 (4) (2022) 4571–4587.

[14] M. Chen, W. Chen, H. Zhong, D. Chi, Y. Wang, M. Zhang, Experimental study on dynamic compressive behaviour of recycled tyre polymer fibre reinforced concrete, Cem. Concr. Compos. 98 (2019) 95–112.

[15] D.- Yoo, N. Banthia, High-performance strain-hardening cementitious composites with tensile strain capacity exceeding 4%: a review, Cem. Concr. Compos. (2022) 125.

[16] L. Zheng, X. Sharon Huo, Y. Yuan, Experimental investigation on dynamic properties of rubberized concrete, Construct. Build. Mater. 22 (5) (2008) 939–947.

[17] J. Ye, C. Cui, J. Yu, K. Yu, J. Xiao, Fresh and anisotropic-mechanical properties of 3D printable ultra-high ductile concrete with crumb rubber, Compos. B Eng. (2021) 211.

[18] X. Sun, S. Wu, J. Yang, R. Yang, Mechanical properties and crack resistance of crumb rubber modified cement-stabilized macadam, Construct. Build. Mater. (2020) 259.

[19] H.Z. Writing-review, V. Cheng Wei Software, Investigation of freeze-thaw mechanism for crumb rubber concrete by the online strain sensor, Measurement 174 (2021 Apr 1), 109080.

[20] X. Zhu, C. Miao, J. Liu, J. Hong, Influence of crumb rubber on frost resistance of concrete and effect mechanism, Procedia Eng. 27 (2012) 206–213.

[21] S. Parveen, S. Rana, R. Fangueiro, A review on nanomaterial dispersion, microstructure, and mechanical properties of carbon nanotube and nanofiber reinforced cementitious composites, J. Nanomater. 2013 (2013).

[22] J. Shao, H. Zhu, B. Zhao, S.I. Haruna, G. Xue, W. Jiang, et al., Combined effect of recycled tire rubber and carbon nanotubes on the mechanical properties and microstructure of concrete, Construct. Build. Mater. (2022) 322.

[23] B. Han, S. Sun, S. Ding, L. Zhang, X. Yu, J. Ou, Review of nanocarbon-engineered multifunctional cementitious composites, Compos Part A Appl Sci Manuf 70 (2015) 69–81.

[24] E.W. Wong, P.E. Sheehan, C.M. Lieber, Nanobeam mechanics: elasticity, strength, and toughness of nanorods and nanotubes, Science 277 (5334) (1997) 1971–1975.

[25] M.- Yu, O. Lourie, M.J. Dyer, K. Moloni, T.F. Kelly, R.S. Ruoff, Strength and breaking mechanism of multiwalled carbon nanotubes under tensile load, Science 287 (5453) (2000) 637–640.

[26] J. Xu, S. Ashraf, S. khan, X. Chen, A. Akbar, F. Farooq, Micro-cracking pattern recognition of hybrid CNTs/GNPs cement pastes under three-point bending loading using acoustic emission technique, J. Build. Eng. (2021) 42.

[27] Y. Lin, H. Du, Graphene reinforced cement composites: a review, Construct. Build. Mater. (2020) 265.

[28] J. Shao, H. Zhu, B. Zhao, S.I. Haruna, G. Xue, W. Jiang, et al., Combined effect of recycled tire rubber and carbon nanotubes on the mechanical properties and microstructure of concrete, Construct. Build. Mater. (2022) 322.

[29] H. Lu, Y. Yao, Spalling mechanism of carbon nanotube concrete at elevated temperature, Construct. Build. Mater. (2022) 314.

[30] A. Carpinteri, Stability of fracturing process in RC beams, J. Struct. Eng. 110 (3) (1984) 544–558.

[31] D.G. Aggelis, T. Shiotani, S. Momoki, A. Hirama, Acoustic emission and ultrasound for damage characterization of concrete elements, ACI Mater. J. 106 (6) (2009) 509–514.

[32] M. Ohtsu, Y. Tomoda, Phenomenological model of corrosion process in reinforced concrete identified by acoustic emission, ACI Mater. J. 105 (2) (2008) 194–199.

[33] M. Ohtsu, T. Okamoto, S. Yuyama, Moment tensor analysis of AE for cracking mechanisms in concrete, ACI Struct. J. 95 (2) (1998) 87–95.

[34] S. Ashraf, S. Khan, V.K. Oad, Microcracking monitoring and damage detection of graphene nanoplatelets-cement composites based on acoustic emission technology, Case Stud. Constr. Mater. (2023), e01844.

[35] P. Kot, M. Muradov, M. Gkantou, G.S. Kamaris, K. Hashim, D. Yeboah, Recent advancements in non-destructive testing techniques for structural health monitoring, Appl. Sci. 11 (6) (2021).

[36] D.G. Aggelis, A.C. Mpalaskas, T.E. Matikas, Investigation of different fracture modes in cement-based materials by acoustic emission, Cement Concr. Res. 48 (2013) 1–8.

[37] K. Ohno, M. Ohtsu, Crack classification in concrete based on acoustic emission, Construct. Build. Mater. 24 (12) (2010) 2339–2346.

[38] E. Proverbio, Evaluation of deterioration in reinforced concrete structures by AE technique, Mater. Corros. 62 (2) (2011) 161–169.

[39] T. Kishi, M. Ohtsu, T. Okamoto, M. Shigeishi, S. Yuyama, A Proposed Standard for Evaluating Structural Integrity of Reinforced Concrete Beams by Acoustic Emission, ASTM International, 1999.

[40] H.A. Elfergani, R. Pullin, K.M. Holford, Damage assessment of corrosion in prestressed concrete by acoustic emission, Construct. Build. Mater. 40 (2013) 925–933.

[41] D. Li, et al., Damage analysis of CFRP-confined circular concrete-filled steel tubular columns by acoustic emission techniques, Smart Mater. Struct. 24 (8) (2015), 085017.

[42] D. Aggelis, et al., Acoustic emission characterization of the fracture process in fibre reinforced concrete, Construct. Build. Mater. 25 (11) (2011) 4126–4131.

[43] S. Shahidan, et al., Damage classification in reinforced concrete beam by acoustic emission signal analysis, Construct. Build. Mater. 45 (2013) 78–86.
[44] R. Vidya Sagar, R.V. Prasad, B.K. Raghu, et al., Microcracking and fracture process in cement mortar and concrete: a comparative study using acoustic emission technique, Exp. Mech. 53 (2013) 1161–1175.
[45] A. Carpinteri, G. Lacidogna, G. Niccolini, Damage analysis of reinforced concrete buildings by the acoustic emission technique, J Struct Control Health Monit 18 (6) (2011) 660–673.
[46] R.V. Sagar, B.K.R. Prasad, S.S. Kumar, An experimental study on cracking evolution in concrete and cement mortar by the b-value analysis of acoustic emission technique, Cement Concr. Res. 42 (8) (2012) 1094–1104.
[47] T. Shiotani, Evaluation of progressive failure using AE sources and improved b-value on slope model tests, in: Progress in Acoustic Emission VII, JSNDI., 1994, pp. 529–534.
[48] J.H. Kurz, F. Finck, C.U. Grosse, et al., Stress drop and stress redistribution in concrete quantified over time by the b-value analysis, Struct. Health Monit. 5 (1) (2006) 69–81.
[49] A. Carpinteri, G. Lacidogna, S. Puzzi, From criticality to final collapse: evolution of the "b-value" from 1.5 to 1.0. Chaos, Solitons & Fractals 41 (2) (2009) 843–853.
[50] N.B. Burud, J.M. Chandra Kishen, Application of generalized logistic equation for b-value analysis in fracture of plain concrete beams under flexure, Eng. Fract. Mech. 210 (2019) 228–246.
[51] Q.H. Han, J. Xu, A. Carpinteri, et al., Localization of acoustic emission sources in structural health monitoring of masonry bridge, Struct Control Hlth 22 (2) (2015) 314–329.
[52] T. Alomayri, B. Ali, S.S. Raza, C. El Hachem, H. Ahmed, M. Azab, Effect of matrix strengthening using micro-silica on mechanical and absorption characteristics of HPC reinforced with reclaimed jute fibres, Case Stud. Constr. Mater. (2023), e02085.
[53] M.A. Gulzar, B. Ali, O. Barakat, A.M. Najemalden, A. Salih Mohammed, Y. Alashker, Influence of jute fiber on tensile, electrical, and permeability characteristics of slag concrete: a better, cheaper, and eco-friendly substitute for conventional concrete, J. Nat. Fibers 20 (1) (2023), 2170947.
[54] B. Ali, M. Azab, R. Kurda, N.B. Kahla, M. Atig, A multi-criteria evaluation and optimization of sustainable fiber-reinforced concrete developed with nylon waste fibers and micro-silica, Environ. Sci. Pollut. Control Ser. (2023) 1–9.
[55] S.T. Gillani, K. Hu, B. Ali, R. Malik, A.B. Elhag, K.M. Elhadi, Life cycle impact of concrete incorporating nylon waste and demolition waste, Environ. Sci. Pollut. Control Ser. 1 (1) (2023).
[56] ACI Committee 211 Method of Proportioning Portland Cement Concrete Tables and Guidelines.
[57] I.K. Tragazikis, K.G. Dassios, D.A. Exarchos, P.T. Dalla, T.E. Matikas, Acoustic emission investigation of the mechanical performance of carbon nanotube-modified cement-based mortars, Construct. Build. Mater. 122 (2016) 518–524.
[58] S. Chuah, Z. Pan, J.G. Sanjayan, C.M. Wang, W.H. Duan, Nano reinforced cement and concrete composites and new perspective from graphene oxide, Construct. Build. Mater. 73 (2014 Dec 30) 113–124.
[59] A.S. Standard, Standard Test Method for Static Modulus of Elasticity and Poisson's Ratio of Concrete in Compression, C469/C469M-14, 2014.
[60] S. Ali, M.N. Sheikh, M. Sargeant, M.N. Hadi, Influence of polypropylene and glass fibers on alkali-activated slag/fly ash concrete, ACI Struct. J. (4) (2020 Jul 1) 117.
[61] N. Gong, S. Hu, X. Chen, X. Fan, X. Cai, Fracture behavior and acoustic emission characteristics of reinforced concrete under mixed mode I-II load conditions, Theor. Appl. Fract. Mech. (2020) 109.
[62] Y. Mizutani, K. Nagashima, M. Takemoto, K. Ono, Fracture mechanism characterization of cross-ply carbon-fiber composites using acoustic emission analysis, NDT E Int. 33 (2) (2000) 101–110.
[63] Zhou J. A Study of Acoustic Emission Technique for Concrete Damage Detection.
[64] N.B. Burud, J.M. Chandra Kishen, Application of generalized logistic equation for b-value analysis in fracture of plain concrete beams under flexure, Eng. Fract. Mech. 210 (2019) 228–246.
[65] B. Gutenberg, C.F. Richter, Frequency of earthquakes in California, Bull. Seismol. Soc. Am. 34 (4) (1944) 185–188.
[66] M.A.A. Aldahdooh, N. Muhamad Bunnori, Crack classification in reinforced concrete beams with varying thicknesses by mean of acoustic emission signal features, Construct. Build. Mater. 45 (2013) 282–288.
[67] P. Code, Eurocode 2: Design of Concrete Structures-Part 1–1: General Rules and Rules for Buildings, British Standard Institution, London, 2005 Aug 14.
[68] Aci Committee, ACI 318-19: Building Code Requirements for Structural Concrete and Commentary, American Concrete Institute, Farmington Hills, MI, USA, 2019.
[69] H.G. Russell, A.R. Anderson, J.O. Banning, I.G. Cantor, R.L. Carrasquillo, J.E. Cook, G.C. Frantz, W.T. Hester, K.L. Saucier, P.C. Aitcin, F.D. Anderson, State-of-the-art report on high-strength concrete, ACI Committee 363 (1997) 92.
[70] CSA A23.3-04, Design of Concrete Structures, Canadian Standards Association (CSA), Rexdale, Ontario, 2003.
[71] NS 3473, Concrete Structures, Design Rules, Nor, Counc. Build. Stand. Oslo, Norw, 1989.
[72] M.A. Rashid, M.A. Mansur, P. Paramasivam, Correlations between mechanical properties of high-strength concrete, J. Mater. Civ. Eng. 14 (3) (2002) 230–238.
[73] M. Jalal, N. Nassir, H. Jalal, Waste tire rubber and pozzolans in concrete: a tradeoff between cleaner production and mechanical properties in a greener concrete, J. Clean. Prod. 238 (2019), 11788.